Construction and Building Materials 261 (2020) 119968

Contents lists available at ScienceDirect

Construction and Building Materials

journal homepage: www.elsevier.com/locate/conbuildmat

Crack width evaluation of fiber-reinforced cementitious composite considering interaction between deformed steel rebar

Daiki Sunaga [a,*], Keisuke Namiki [b], Toshiyuki Kanakubo [c]

[a] Graduate School of System and Information Engineering, University of Tsukuba, 1-1-1, Tennohdai, Tsukuba-city, Ibaraki 305-8573, Japan
[b] Graduate School of System and Information Engineering, University of Tsukuba, Ibaraki, Japan
[c] Division of Engineering Mechanics and Energy, University of Tsukuba, Ibaraki, Japan

HIGHLIGHTS

- Uniaxial tension test is conducted for steel-reinforced PVA-FRCC prism specimens.
- The crack opening tends to be smaller with increasing of fiber volume fraction.
- A prediction formula of crack width in steel-reinforced FRCC is newly proposed.
- Bond interaction and fiber bridging effect are considered in the formula.
- The predicted steel strain – crack width relationship fits experimental results.

ARTICLE INFO

Article history:
Received 21 February 2020
Received in revised form 29 April 2020
Accepted 14 June 2020
Available online 29 June 2020

Keywords:
Fiber-reinforced cementitious composite
Polyvinyl alcohol fiber
Crack width
Uniaxial tension test
Bond stress
Bridging stress

ABSTRACT

This study aims to propose a simple evaluation method of crack width in reinforced FRCC members. Uniaxial tension test is conducted for steel-reinforced FRCC prism specimens with slits to measure crack width clearly. The test parameters are cross-sectional size of prism and fiber volume fraction of FRCC. Through the loading test, steel strain – crack width relationship is obtained. The theoretical calculation formula to predict crack width in steel-reinforced FRCC is led by solving the force equilibrium and compatibility conditions between FRCC and reinforcing bar considering bond stress – slip relationship, fiber bridging law (bridging stress – crack width relationship) and condition of crack occurrence. The steel strain – crack width curves predicted by the proposed formula show a good adaptability with the experimental results in each parameter.

1. Introduction

Fiber-reinforced cementitious composite (FRCC) is cementitious material mixed with short discrete fibers into cement matrix to improve brittle behavior of composites especially in tensile and bending field. FRCC shows high ductility because of fiber bridging through cracks and control the crack opening. FRCC has been also expected to bring high durability to reinforced concrete structures by its small opening cracks that prohibit the penetrations of aggressive attacks to deteriorate the internal reinforcing rebars and FRCC itself.

In past several decades, a number of types of FRCC have been introduced and studied by lots of researchers. Steel fibers or polymeric fibers such as polyethylene (PE), polyvinyl alcohol (PVA), and polypropylene (PP) fibers have been utilized in FRCC. While steel fiber-reinforced concrete (SFRC) commonly shows tension-softening behavior after initial cracking, FRCCs which are recently developed and studied show much higher ductility. FRCC showing a deflection hardening behavior under bending condition is defined as ductile fiber-reinforced cementitious composites (DFRCC) [1], while FRCC showing pseudo-strain hardening behavior under the uniaxial tension is defined as strain hardening cementitious composites (SHCC) [2]. The high ductility of these materials is achieved by the bridging effect of individual fibers in the matrix. In DFRCC and SHCC, polymeric fibers are commonly used rather than steel fiber. Engineered cementitious composites (ECC) [3], a class of cementitious materials typically reinforced with PE or PVA fibers, are one of the examples of SHCC materials showing high tensile strain hardening ability. Actual applications have been reported using them for beams, walls, decks and slabs, tunnel linings, concrete substrate retrofitting materials, etc. It has been expected to

* Corresponding author.
E-mail address: s1920914@s.tsukuba.ac.jp (D. Sunaga).

https://doi.org/10.1016/j.conbuildmat.2020.119968
0950-0618/

expand the use of these FRCCs with additional values for resilient and sustainable structures.

It's no exaggeration to say that the advantage of FRCC lies on the controlling of crack width by bridging effect of fibers across the crack. The tensile stress versus crack width relationships (hereafter, called bridging law) can feature the crack width and crack opening behavior of FRCC itself and have been studied by many researchers. In general, bridging law of FRCC can be directly obtained from a uniaxial tension test [4,5], or alternatively, indirectly from a prism bending test [6]. However, in SHCC, it is difficult to measure the crack opening of single crack because of the multiple cracking behavior. To solve this problem, Pereira et al. have proposed the unique testing method using 0.5 mm thick notched specimen [7] and Yu et al. have proposed the high-precision measuring method of crack opening using Digital Image Processing [8].

On the other hand, the micromechanical modeling of bridging law of steel and PP fiber-reinforced concrete was first introduced by Li et al. [9]. Tensile stress can be given by the function of crack opening that is featured by the slip-out behavior of the individual fibers considering the effect of the inclined angle and probability density function for fiber dispersion and orientation. Especially in SFRC, bridging law has been studied theoretically by some researchers (e.g. [10]). Furthermore, Yang et al. have updated the micromechanical bridging law model for PVA-ECC by including strain-hardening behavior [11]. The authors have also studied bridging law for PVA-FRCC [12] and Aramid-FRCC [13]. The both calculated bridging laws show good agreements with the results of uniaxial tension test. In PVA-FRCC, the calculated bridging laws have been expressed by tri-linear model by also the authors [14], in which the characteristics points of tri-linear model have been given by the function of fiber orientation intensity.

FRCC is generally utilized with steel reinforcing rebars in actual structures similarly as conventional concrete structures. As well known, crack width in conventional concrete structures is affected not only by the characteristics of concrete but also by reinforcement ratio and interaction between concrete and rebars. For conventional concrete, the authors have proposed a crack width prediction method led by calculation of bond interactions [15]. The crack width is expressed by a simple function of dimensions of concrete prism and rebar, bond stiffness, tensile strength of concrete, and strain of rebar. For FRCC, in fact, some researchers have conducted uniaxial tension test of steel-reinforced FRCC prisms and evaluated cracking behavior [16–18]. In addition to these experimental studies, Ogura et al. have conducted tensile fracture analysis of FRCC with the rebar and evaluated load carrying capacity, deformation performance and crack propagation behavior [19]. Though the crack width of FRCC itself can be obtained through bridging law, it is considered that crack width in steel-reinforced FRCC is also affected by the interaction between rebars. Some researchers have studied theoretical calculations of crack width in FRCC with conventional reinforcement considering both the interaction of steel deformed rebar and fiber bridging effect at cracks [20,21]. However, these methodologies are complicated and require convergence calculations to solve. It is quite convenience in the practical structures' design to calculate crack width by a simple formula in which the crack width is expressed using the stress or strain of rebars.

This study aims to propose a simple evaluation method of crack width in steel-reinforced FRCC. Uniaxial tension test is firstly conducted for steel-reinforced FRCC prism specimens with slits and crack width is measured experimentally. After that, theoretical calculation of bond interactions considering bridging effect of fibers at crack is conducted to propose a prediction method of crack width of steel-reinforced FRCC.

2. Outline of uniaxial tension test

2.1. Specimens

Fig. 1 shows the dimensions of specimens and Table 1 shows the list of specimens. The specimen is FRCC prism with square cross section and its total length is 600 mm. One steel deformed rebar D16 (SD490: specific yield strength of 490 MPa) was arranged in the center of cross section along the axial direction. PVA fibers were used for FRCC. The experimental parameters are cross-sectional size and fiber volume fraction. The cross section was set to 100 mm, 120 mm, and 140 mm square for A, B, and C series of specimens, respectively. To control the cracking position, slits were set on both sides of specimen spaced at 100 mm. The depth of silt was changed in accordance with the cross-sectional size as the cross-sectional area at the slit position was reduced to 60% area of full section. In order not to affect the fiber orientation, the slits were installed after demolding using a concrete cutter. Fiber volume fraction was set to 0% (mortar), 1%, and 2%. Three specimens were tested for each combination of test parameters.

2.2. Materials

Table 2 shows the dimensions and mechanical properties of PVA fiber used in FRCC and Fig. 2 shows the visual appearance of the fiber. PVA fiber with diameter of 0.1 mm and 12 mm length was utilized. This PVA fiber is same one used in the previous studies [12,14] conducted by the authors. Table 3 shows the mixture proportion and mechanical properties of FRCC. The mixture proportion is also same one designed in the previous studies [12,14] conducted by the authors. Compression test for FRCC was carried out at the same time with the tension test using ϕ100mm $\times$ 200 m m cylinder test pieces. Fresh FRCC is filled into the mold by pouring from one end of the mold to pay attention controlling the fiber orientation. Table 4 shows the mechanical properties of reinforcing bar. Steel deformed reinforcing bar with nominal diameter of 16 mm and specific yield strength of 490 MPa was utilized.

2.3. Loading and measurements

Fig. 3 shows the test setup. Uniaxial tension test was conducted by the universal testing machine. Crack width at each slit position was measured by Pi-type linear variable displacement transducers (LVDTs) spaced at 100 mm on both side of the specimens. The total deformation was measured by two LVDTs to observe the yielding of steel rebar.

3. Test results

3.1. Crack patterns

Fig. 4 shows the examples of crack patterns after steel rebar yielding. The specimens showing less cracks in axial direction are picked up from each series of specimens. Cracks took place at slit positions before steel rebar yielding in all specimens. However, branched cracks at slit positions were observed in many specimens. In addition, some cracks took place at no-slit position. The number of cracks at no-slit position decreased with increasing of sectional size.

3.2. Steel strain – crack width relationships

The crack width is calculated by averaging two values measured by both sides of Pi-type LVDTs in the case of a single crack at the slit. After observing the branched crack or occurring the second

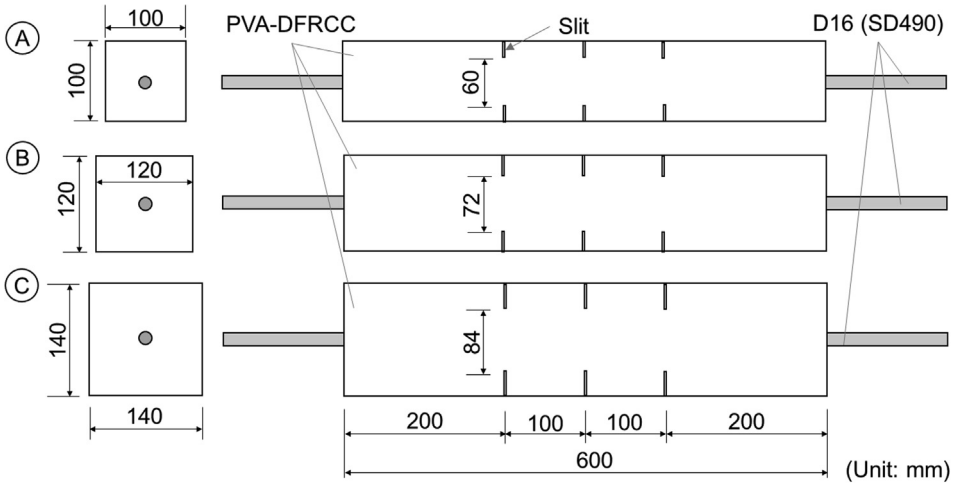

Fig. 1. Dimension of specimens.

Table 1
List of specimens.

Type	ID	Common factor	Cross-sectional size (sectional size at slit)	Volume fraction of fibers
No Fiber-A	1 ~ 3	Length: 600 mm	100 mm × 100 mm	–
PVA1%-A	1 ~ 3	Number of slits: 6	(100 mm × 60 mm)	1.0%
PVA2%-A	1 ~ 3	Spacing of slits: 100 mm		2.0%
No Fiber-B	1 ~ 3	Steel rebar: D16 (SD490)	120 mm × 120 mm	–
PVA1%-B	1 ~ 3	Fiber: PVA	(120 mm × 72 mm)	1.0%
PVA2%-B	1 ~ 3			2.0%
No Fiber-C	1 ~ 3		140 mm × 140 mm	–
PVA1%-C	1 ~ 3		(140 mm × 84 mm)	1.0%
PVA2%-C	1 ~ 3			2.0%

Table 2
Mechanical properties of fiber.

Fiber	Length (mm)	Diameter (mm)	Tensile strength (MPa)	Elastic modulus (GPa)
PVA	12	0.10	1200	28

Fig. 2. Visual appearance of fiber.

crack in the measurement region, the measured crack width was excluded from the evaluation. Tension load is converted to steel strain by using the elastic modulus obtained from the tension test of reinforcing bars (Table 4).

Fig. 5 shows the steel strain – crack width relationship. The test results of each slit position in the same series of specimens are shown in the same graph. The dotted line in Fig. 5 shows the average of test results in each series of specimens. The test results of each slit position are approximated with proportional relations ($y = ax$) by using the least square method and the average lines are determined by averaging these coefficients, a.

According to the test results, larger fiber volume fraction leads an increment of the coefficients comparing among No Fiber, PVA 1% and 2% specimens in B and C series. Crack opening tend to be smaller with increasing of fiber volume because the fiber bridging

Table 3
Mixture proportion and mechanical properties of FRCC.

Type	Unit weight (kg/m^3)					Compressive strength (MPa)	Elastic modulus (GPa)
	Water	Cement	Sand	Fly ash	PVA fiber		
No Fiber	380	678	484	291	0	52.5	18.1
PVA1%	380	678	484	291	13	49.5	17.6
PVA2%	380	678	484	291	26	41.2	15.6

Table 4
Mechanical properties of reinforcing bar.

Type	Yield strength (MPa)	Elastic modulus (GPa)	Yield strain (μ)	Tensile strength (MPa)
D16 (SD490)	516	198	2604	709

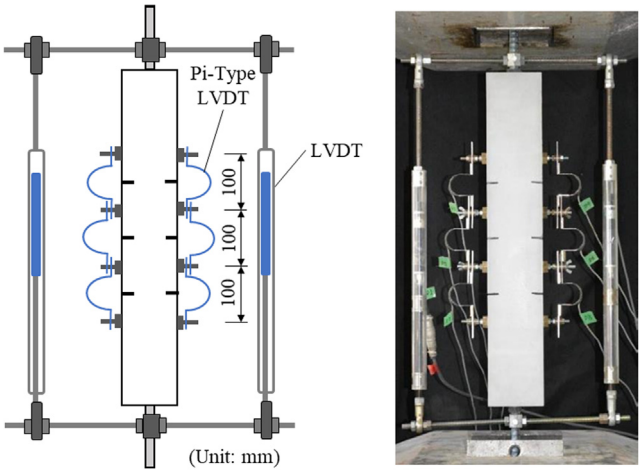

Fig. 3. Test setup.

force at crack increases. No large difference is observed among A series specimens because of smaller cross-sectional area in which fibers bridge the crack.

On the other hand, in comparison among A, B, and C series in no-fiber specimens, increasing of sectional size causes decreases of the slop of the average lines. Since the number of cracks decreases with increasing of cross-sectional area, crack opening tends to be larger at the same strain of steel rebar. In the case of PVA1% and 2% specimens, the influence of sectional size is less than the case of no-fiber specimens because of the effect of fiber bridging.

4. Theoretical solution of crack width

In previous study [15], theoretical solution of crack width in steel-reinforced concrete member have been obtained based on the equilibrium and compatibility conditions considering the bond interaction between concrete and rebar. The crack width is given by the function of the strain of rebar. In this study, same theoretical procedure is conducted in streel reinforced FRCC member involving the bridging effect of fibers at crack. The relationship between strain of reinforcing bar and crack width is obtained from the equilibrium of axial forces and compatibility conditions in infinitesimal element of reinforced FRCC.

Fig. 6 shows the infinitesimal element of reinforced FRCC under tensile condition. Where, dx is length of the infinitesimal element, P_{sx} is tensile load of rebar, dP_{sx} is increment of tensile load of rebar in dx, τ_x is bond stress, s_x is slip and ds_x is increment of slip in dx. Eq. (1) gives the definition of bond stress which is obtained from the force equilibrium of rebar in axial direction.

$$\frac{dP_{sx}}{dx} = \tau_x \cdot \varphi_s \tag{1}$$

where φ_s is perimeter of rebar. Assuming that the rebar behaves in elastic manner, tensile force of rebar is expressed by strain as Eq. (2).

$$\frac{d\varepsilon_{sx}}{dx} = \frac{\varphi_s}{E_s A_s} \cdot \tau_x \tag{2}$$

where, ε_{sx} is strain of rebar, E_s is elastic modulus of rebar, and A_s is cross-sectional area of rebar. Since the slip is defined as difference of deformation between rebar and surrounding FRCC, Eq. (3) is obtained from compatibility condition in the infinitesimal element.

$$\frac{ds_x}{dx} = \varepsilon_{sx} - \varepsilon_{cx} \tag{3}$$

where ε_{cx} is strain of FRCC.

A reinforced FRCC prism which is subjected to uniaxial tensile load is shown in Fig. 7. Cracks occur in the prism by increasing the tensile load at loaded end, $P_{s(LOAD)}$. Uncracked region between two cracks is focused and x-axis is defined in axial direction of the prism as the origin positions at the center of the uncracked region (x = 0). The half-length of the uncracked region is defined as l so that the crack locates at $x = l$. P_{sx} and P_{cx} represent tensile

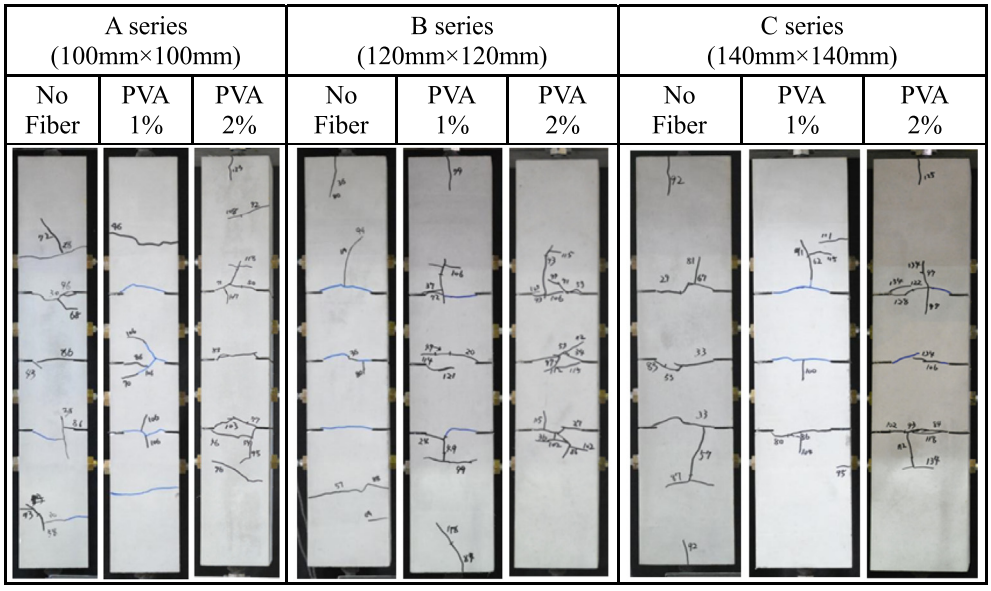

Fig. 4. Examples of crack patterns after yielding of steel rebar.

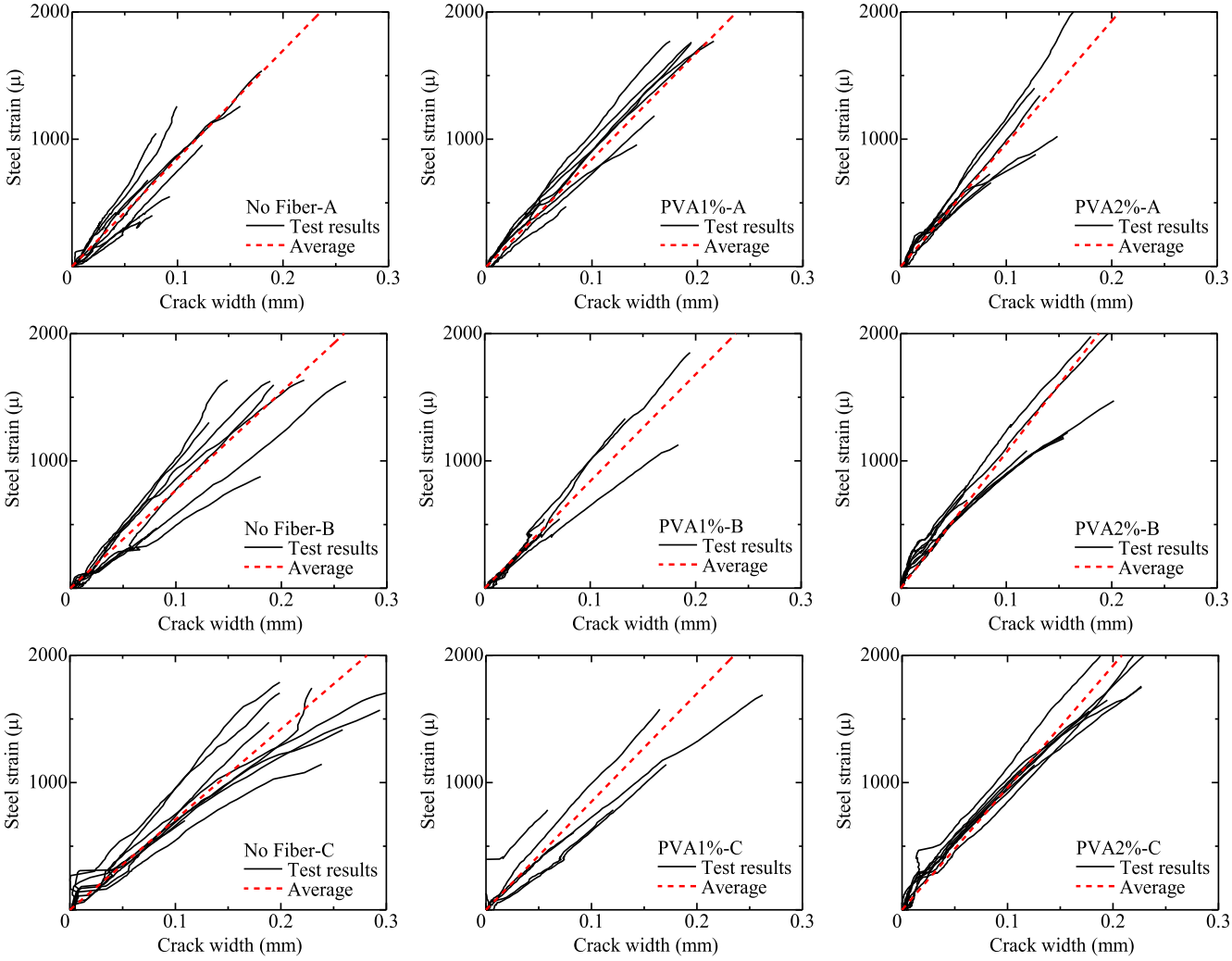

Fig. 5. Steel strain – crack width relationship.

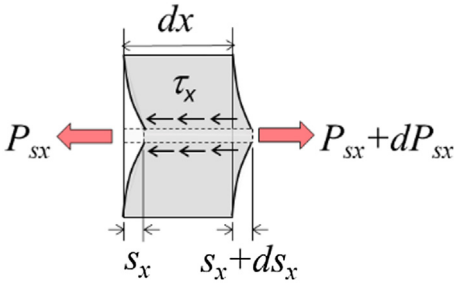

Fig. 6. Infinitesimal element of reinforced FRCC under tensile condition.

forces of rebar and that of FRCC at arbitrary position in the uncracked region, x, respectively. At the crack in reinforced FRCC, tensile force is transferred not only by the rebar, P_{sl}, but also by the bridging of fibers, P_{br}. Eq. (4) gives the equilibrium condition of axial forces. Eq. (4) leads Eq. (5) assuming that the rebar and FRCC in the uncracked region remains in elastic.

$$P_{sx} + P_{cx} = P_{sl} + P_{br} (= P_{s(LOAD)}) \tag{4}$$

$$np\varepsilon_{sx} + \varepsilon_{cx} = np\varepsilon_{sl} + \frac{1}{E_c}\sigma_{br} (= np\varepsilon_{s(LOAD)}) \tag{5}$$

where,

σ_{br}: fiber bridging stress at crack (=P_{br}/A_c),
ε_{sl}: strain of rebar at crack,
$\varepsilon_{s(LOAD)}$: strain of rebar at loaded end,
n: ratio of elastic modulus (=E_s/E_c),
p: reinforcement ratio (=A_s/A_c),
E_s: elastic modulus of rebar,
E_c: elastic modulus of FRCC,
A_s: cross-sectional area of rebar,
A_c: cross-sectional area of FRCC.

Substituting Eq. (5) for Eq. (3), Eq. (6) is obtained. Eq. (2) and Eq. (6) lead Eq. (7).

$$\frac{ds_x}{dx} = (1 + np) \cdot \varepsilon_{sx} - np \cdot \varepsilon_{sl} - \frac{1}{E_c}\sigma_{br} \tag{6}$$

$$\frac{d\varepsilon_{sx}}{ds_x} = \frac{\varphi_s}{E_s A_s} \cdot \frac{\tau_x}{(1+np)\cdot\varepsilon_{sx} - np\cdot\varepsilon_{sl} - \frac{1}{E_c}\sigma_{br}} \tag{7}$$

Integration of Eq. (7) from the center (x = 0) to crack position (x = l) is expressed by Eq. (8).

$$\int_{\varepsilon_{s0}}^{\varepsilon_{sl}} \{(1 + np) \cdot \varepsilon_{sx} - np \cdot \varepsilon_{sl} - \frac{1}{E_c}\sigma_{br}\} d\varepsilon_{sx} = \int_{s_0}^{s_l} \frac{\varphi_s}{E_s A_s} \cdot \tau_x ds_x \tag{8}$$

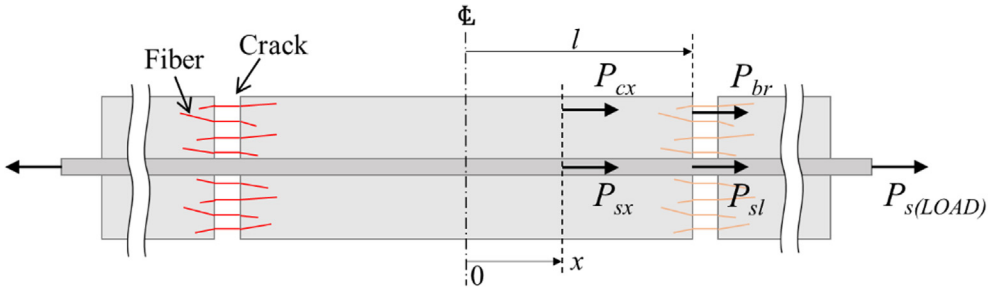

Fig. 7. Cracked reinforced FRCC prism in tension.

where,

ε_{s0}: strain of rebar at $x = 0$,
s_0: slip at $x = 0$,
s_l: slip at $x = l$.

Slip at $x = 0$, i.e., relative displacement between rebar and FRCC at the center of uncracked region can be assumed to be zero ($s_0 = 0$) because of the symmetric condition. Integral calculus of Eq. (8) gives Eq. (9).

$$\frac{1+np}{2}\left(\varepsilon_{sl}{}^2 - \varepsilon_{s0}{}^2\right) - (np\cdot\varepsilon_{sl} + \frac{1}{E_c}\sigma_{br})(\varepsilon_{sl} - \varepsilon_{s0}) = \frac{\varphi_s}{E_sA_s}\int_0^{s_l}\tau_x ds_x \tag{9}$$

Eq. (9) gives the fundamental relationships between strains of rebar (ε_{s0} and ε_{sl}) and slip at crack (s_l). To achieve the goal of this study, it is convenience that the slip at crack can be expressed only by the strain of rebar at crack. An additional condition is introduced to eliminate the term of ε_{s0}.

Tensile stress in FRCC becomes the largest at the center ($x = 0$) in uncracked region due to transmitted stress from rebar via bond stress. When tensile force of rebar increases, a new crack in FRCC is generated at the center of uncracked region resulting that the uncracked region is separated into two parts. The slip at crack which locates the end of uncracked region shows largest value just at the generation of the new crack. This condition means that the slip at crack is maximized when tensile stress in FRCC at the center reaches its cracking strength. This condition leads Eq. (10), where σ_{cr} is cracking strength of FRCC. Eq. (10) expresses that tensile strength at cracking in FRCC has the equilibrium with the bridging force at crack and the increment force by bond stress.

$$\sigma_{cr}A_c = \varphi_s\cdot\int_0^l \tau_x dx + \sigma_{br}A_c \tag{10}$$

Substituting Eq. (2) for Eq. (10), Eq. (11) is derived. Eq. (11) is calculated as Eq. (12).

$$\sigma_{cr}A_c = E_sA_s\int_0^l \frac{d\varepsilon_{sx}}{dx}dx + \sigma_{br}A_c = E_sA_s\int_{\varepsilon_{s0}}^{\varepsilon_{sl}} d\varepsilon_{sx} + \sigma_{br}A_c \tag{11}$$

$$\sigma_{cr}A_c = E_sA_s\cdot(\varepsilon_{sl} - \varepsilon_{s0}) + \sigma_{br}A_c \tag{12}$$

Substituting Eq. (12) for Eq. (9), strain of rebar at crack position, ε_{sl}, is given by Eq. (13).

$$\varepsilon_{sl} = \frac{\varphi_s}{A_c(\sigma_{cr}-\sigma_{br})}\int_0^{s_l}\tau_x ds_x + \frac{1}{E_c}\sigma_{br} + \frac{1+np}{2npE_c}(\sigma_{cr} - \sigma_{br}) \tag{13}$$

Eq. (13) expresses the relationship between strain of rebar and slip at crack position when a new crack generates. Since crack width of FRCC can be considered to involve the slips from the both sides of uncracked regions, it can be assumed that the slip at the crack position gives half of crack width. So, Eq. (13) gives the relationship between strain of rebar at crack position and crack width which has the possibility to become the maximum.

Eq. (13) is adaptable for the materials in elastic manner in tension and with any relations between bond stress and slip. However, bond stress should be given by function of slip to solve Eq. (13). As previously mentioned, FRCC shows small crack opening. In this study, since the target range of slip (half of crack width) is enough small such as less than 0.2 mm, bond stress versus slip relations is assumed to be given by elastic model. This assumption also helps to obtain mathematical solution by easy form for the practical use. The model is defined by bond stiffness, k_{bo}, as given in Eq. (14).

$$\tau_x = k_{bo}\cdot s_x \tag{14}$$

Using Eq. (14), integral calculus for bond stress in Eq. (13) is derived as Eq. (15).

$$\int_0^{s_l}\tau_x ds_x = \frac{1}{2}k_{bo}\cdot s_{sl}{}^2 \tag{15}$$

Substituting Eq. (15) for Eq. (13), and assuming that crack width, w_{cr}, is equal to two times slip at crack position, Eq. (16) is derived.

$$\varepsilon_{sl} = \frac{k_{bo}\varphi_s}{8A_c(\sigma_{cr}-\sigma_{br})}w_{cr}{}^2 + \frac{1}{E_c}\sigma_{br} + \frac{1+np}{2npE_c}(\sigma_{cr} - \sigma_{br}) \tag{16}$$

It can be considered that fiber bridging stress, σ_{br}, has also relations with crack width. The valuation of fiber bridging characteristics is one of the most essential topics for discussing performance of FRCC in tension. According to the results of our previous studies [12,14], crack bridging stress of fibers in FRCC, σ_{br}, is given by the function of crack width, w_{cr}. Therefore, Eq. (16) can be expressed as follows.

$$\varepsilon_{sl} = \frac{k_{bo}\varphi_s}{8A_c\{\sigma_{cr}-\sigma_{br}(w_{cr})\}}w_{cr}{}^2 + \frac{1}{E_c}\sigma_{br}(w_{cr}) + \frac{1+np}{2npE_c}\{\sigma_{cr} - \sigma_{br}(w_{cr})\} \tag{17}$$

Eq. (17) gives the relationship between strain of rebar at crack position and crack width when a new crack generates at the center of uncracked region. The crack width given by this relationship is corresponding to the maximum value for the following reasons.

Fig. 8 shows the schematic drawings of rebar strain – crack width relationship expressed by Eq. (17). The dotted lines in Fig. 8 shows the examples of crack opening behavior of a certain crack. When the crack width reaches to the theoretical value with increasing of steel strain, new crack generates at the center of uncracked region. That is because this formula is led by using condition that tensile stress at the center of uncracked FRCC reaches to the cracking strength. This phenomenon causes the increasing of the number of cracks, hence, the crack width of each crack decreases because crack width is given as total deformation of specimen divided by the number of cracks. For this reason, crack opening of a certain crack does not exceed the theoretical value. Therefore, it can be said that this formula gives the possible maximum crack width at arbitrary strain of rebar. As the feature of this formula, crack spacing (=two times bond length) is not required for the calculation.

Here, to compare the calculations by Eq. (17) with the test results, equilibrium of the axial force between crack position and loaded end is considered as previously shown in Fig. 7. As seen in Eq. (18), the summation of tensile force of steel rebar at crack position, P_{sl}, and fiber bridging force, P_{br}, is equal to the tensile

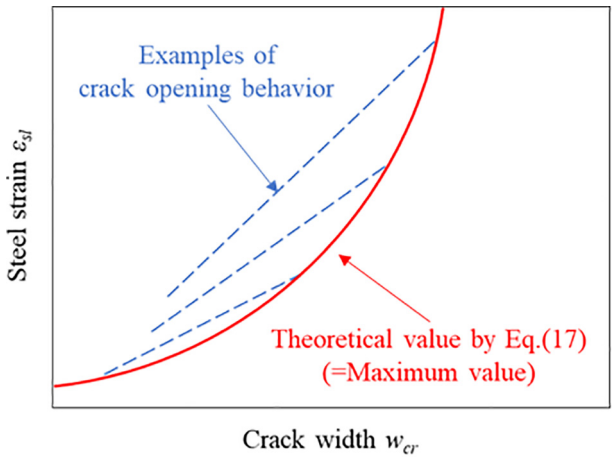

Fig. 8. Rebar strain – crack width relationship expressed by Eq. (17).

force of steel rebar at loaded end, $P_{s(LOAD)}$. Note that, $P_{s(LOAD)}$ is corresponding to the test load of uniaxial tension test.

$$P_{sl} + P_{br} = P_{s(LOAD)} \tag{18}$$

In the case of conventional concrete, since the fiber bridging effect at cracks does not exist and P_{br} is equal to zero, tensile force of rebar at loaded end, $P_{s(LOAD)}$, is the same as that at crack position, P_{sl}. On the other hand, in the case of FRCC, tensile force of rebar at crack, P_{sl}, is smaller than that at loaded end, $P_{s(LOAD)}$, because of the bridging effect of fibers, P_{br}. The relationship between the forces at crack and at loaded end is expressed as Eq. (19) by using stain of rebar at crack position, ε_{sl}, at loaded end, $\varepsilon_{s(LOAD)}$, and fiber bridging stress, σ_{br}.

$$\varepsilon_{sl} + \frac{1}{npE_c}\sigma_{br} = \varepsilon_{s(LOAD)} \tag{19}$$

While the steel strain shown in Fig. 5 which is obtained from uniaxial tension test is corresponding to $\varepsilon_{s(LOAD)}$, the steel strain given by Eq. (17) is corresponding to ε_{sl}. Therefore, the test results cannot be directly compared with the theoretical results obtained from Eq. (17). However, it is difficult to measure the steel strain at crack position in uniaxial tension test. To solve this problem, theoretical formula which is expressed by $\varepsilon_{s(LOAD)}$ instead of ε_{sl} is also derived as Eq. (20) by substituting Eq. (17) to Eq. (19).

$$\varepsilon_{s(LOAD)} = \frac{k_{bo}\varphi_s}{8A_c\{\sigma_{cr}-\sigma_{br}(w_{cr})\}} w_{cr}^{\,2} + \frac{1+np}{2npE_c}\{\sigma_{cr} + \sigma_{br}(w_{cr})\} \tag{20}$$

Eq. (20) gives the relationship between strain of rebar at loaded end and crack width when a new crack generates. In the next chapter, theoretical results obtained by Eq. (20) is compared with the test results obtained in Chapter 3 and the adaptability of this theoretical solution is confirmed.

5. Adaptability of proposed method

5.1. Used parameters and constitutive laws in theoretical formula

The adaptability of the proposed method to predict the crack width in steel-reinforced FRCC prisms is evaluated in this chapter comparing with the experimental results.

Table 5 shows the used parameters in theoretical formula, Eq. (20). The nominal values are used in cross-sectional area and perimeter of steel rebar. Sectional size of FRCC agrees with the dimensions of specimens described in Chapter 2. The elastic modulus of steel rebar and FRCC is obtained from material tests explained in Chapter 2.

Cracking strength of FRCC is calculated from the test results of uniaxial tension test because it is difficult to obtain the value directly from the material test. According to the steel strain – crack width relationships of C series specimens shown in Fig. 5, rapid increasing of crack width is observed in the small range of steel strains. It is considered that the cracks start opening at those steel

Table 5
Used parameters in theoretical formula.

				No Fiber	PVA 1%	PVA 2%	Reference
Steel rebar	Cross-sectional area	A_s	mm^2		198.6		Nominal value
	Perimeter	φ_s	mm		50		Nominal value
	Elastic modulus	E_s	GPa		198		Material test
FRCC	Cross-sectional area	A_c	mm^2		A:100^2, B:120^2, C:140^2		Dimension
	Elastic modulus	E_c	GPa	18.1	17.6	15.6	Material test
	Cracking strength	σ_{cr}	MPa	1.03	1.33	1.56	Fig. 5

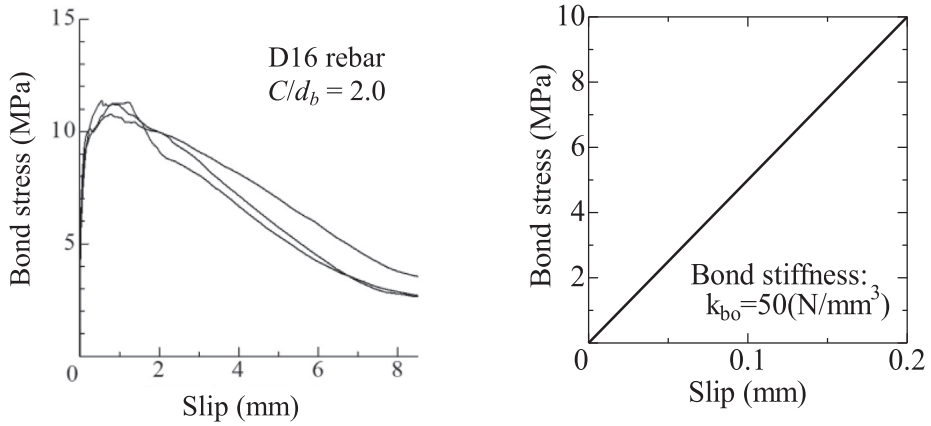

Fig. 9. Bond stress versus slip relation (left: examples of test results [22], right: model).

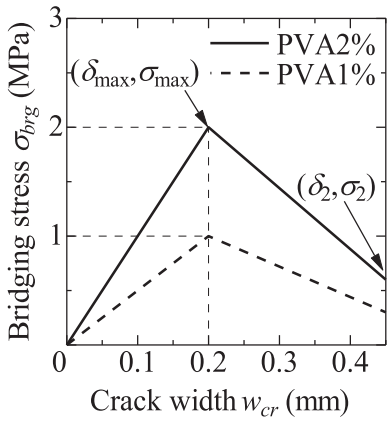

Fig. 10. Bridging law.

strains. The values are 324μ, 420μ and 492μ in No Fiber, PVA1% and 2% specimens, respectively. These values are converted to the tensile load by using elastic modulus and cross-sectional area of steel rebar. The tensile loads are divided by the cross-sectional area of FRCC at slit position (140 mm × 84 mm) and cracking strength is calculated as shown in Table 5.

Bond stress versus slip relation is assumed from the test result of steel rebar pullout test using PVA-ECC [22] which compressive strength is almost the same as FRCC used in this study. Based on the test result of PVA-ECC specimens reinforced with D16 rebar and cover thickness of 32 mm, bond stiffness is assumed as k_{bo} = 50-N/mm^3 and bond stress – slip relationship is modeled as shown in Fig. 9.

In previous study [14], the bridging law of FRCC with PVA2% is proposed as tri-linear model. The maximum point (δ_{max}, σ_{max}) and second folding point (δ_2, σ_2) are given by function of fiber orientation intensity, k, as follows.

$$\delta_{max} = 0.20k^{0.18}(\text{mm}) \tag{21}$$

$$\sigma_{max} = 2.0k^{0.30}(\text{MPa}) \tag{22}$$

$$\delta_2 = 0.45(\text{mm}) \tag{23}$$

$$\sigma_2 = 0.60k^{0.73}(\text{MPa}) \tag{24}$$

According to the previous study on size effect of FRCC [23], bending characteristic of PVA-FRCC prism specimen which sectional size is 100 mm × 100 mm can be evaluated by assuming k = 1 in bridging law. Assuming k = 1 corresponds to random orientation of fibers. In this study, k = 1 is also used for bridging law and bi-linear model until δ_2 = 0.45 mm is used as shown in Fig. 10. In FRCC specimens with PVA1%, it is considered that bridging effect is half as much as PVA2% and bridging law is modeled as dotted line shown in Fig. 10. Bridging stress is multiplied by 0.6, which is the ratio of cross-sectional area of FRCC at slit to that of whole

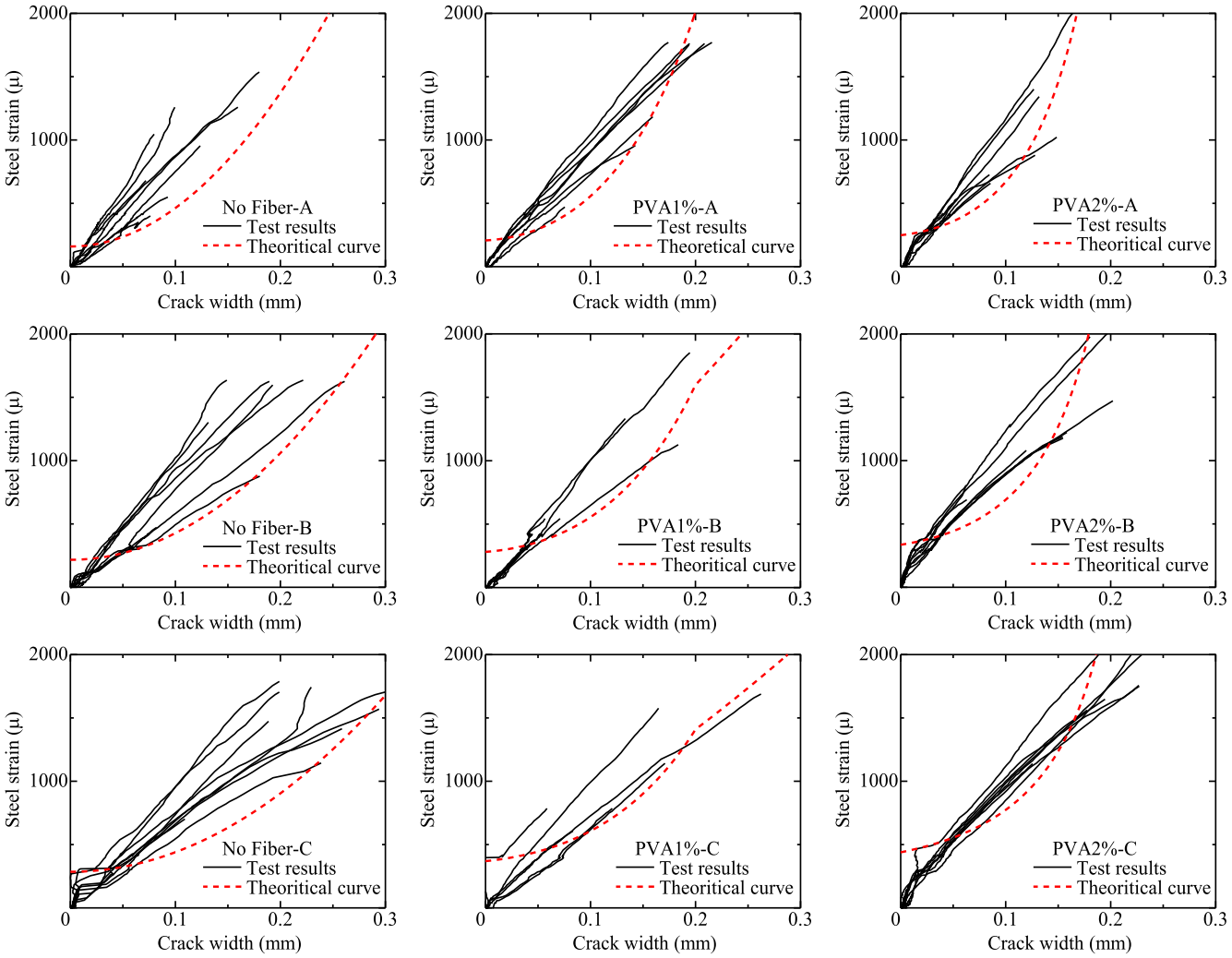

Fig. 11. Steel strain at loaded end – crack width relationships.

section, taking the effect of reducing bridging force at the slit into account. In No Fiber specimens, bridging stress is substituted by zero in the formula.

5.2. Comparison between the calculated result by the formula and the test results

Fig. 11 shows the steel strain at loaded end – crack width relationships obtained from both uniaxial tension tests and theoretical formula, Eq. (20). While the test results show the crack opening of each crack, theoretical curve shows the possible maximum crack width as previously mentioned in Chapter 4. Some theoretical curves show folding point varying the slope of the curve at crack width = 0.2 mm (There is no folding point in no-fiber specimens). This is because the fiber bridging model has the folding point at crack width = 0.2 mm as shown in Fig. 10.

The curves of measured crack widths in most of the specimens locate in the area of smaller crack width than the theoretical curves. It can be said that the theoretical formula shows a good adaptability with the experimental results. The crack widths of some test results exceed the theoretical curve in PVA2%-B and C specimens. In this study, fiber orientation intensity is assumed to be $k = 1$ regardless of sectional size of the specimen. It has been reported that the sectional size affects fiber orientation intensity and fiber bridging stress of bridging law [23]. It is considered that bridging effect is overestimated, and crack width is underestimated in theoretical formula especially in the specimens with much fibers.

In this chapter, the adaptability of the proposed method to predict the crack width in steel-reinforced FRCC prism is confirmed by comparing the steel strain at loaded end – crack width relationship obtained from both theoretical formula, Eq. (20), and uniaxial tension test. It can be said that Eq. (17) which expresses the relationship between steel strain at crack position and crack width is also adoptable in actual members.

If it is considered to use the proposed theoretical solution in the practical structures' design, crack width can be predicted from steel strain at crack position by using Eq. (17). However, since this methodology consists of several assumption, the following points should be paid attention to adapt this solution:

- The bridging law of used fibers should be given by a simple function of crack width to solve the theoretical formula.
- Since only uniaxial stress field is considered in derivation of the formula, the crack width cannot be evaluated under biaxial stress field such as shear stress.
- Since the theoretical solution is derived based on the assumption that the fiber dispersion is uniform along the uniaxial direction of specimen and the crack opening of each crack is the same, the localization of crack opening cannot be evaluated in this solution.

6. Conclusion

To evaluate crack width in reinforced FRCC members, uniaxial tension test is conducted for steel-reinforced FRCC prism specimens and crack width is measured experimentally. Theoretical calculation formulas to predict crack width of reinforced FRCC member is proposed based on the fundamental relations between strain of rebar and slip in FRCC considering bond interaction and bridging stress of fibers. The predicted steel strain – crack width curve shows a good adaptability with the experimental results.

CRediT authorship contribution statement

Daiki Sunaga: Conceptualization, Methodology, Investigation, Formal analysis, Writing - original draft. **Keisuke Namiki:** Investigation. **Toshiyuki Kanakubo:** Conceptualization, Supervision, Writing - review & editing.

Declaration of Competing Interest

The authors declare that they have no known competing financial interests or personal relationships that could have appeared to influence the work reported in this paper.

Acknowledgement

This study was supported by the Japan Society for the Promotion of Science KAKENHI Grant Number 18H03802.

References

[1] T. Matsumoto, H. Mihashi ,JCI-DFRCC Summary Report on DFRCC Terminologies and Application Concepts, Proceedings of the JCI International Workshop on Ductile Fiber Reinforced Cementitious Composites (DFRCC), (2002) 59–66.
[2] K. Rokugo, T. Kanda, eds., Strain Hardening Cement Composites: Structural Design and Performance, RILEM State-of-the-Art Reports 6, (2013).
[3] V.C. Li, Engineered Cementitious Composites (ECC) - Bendable Concrete for Sustainable and Resilient Infrastructure, Springer-Verlag GmbH, Germany, 2019.
[4] I. Löfgren, Fiber-Reinforced Concrete for Industrial Construction – A Fracture Mechanics Approach to Material Testing and Structural Analysis, PhD thesis, Department of Civil and Environmental Engineering, Chalmers University of Technology, Gothenburg, Sweden (2005).
[5] P.N. Balaguru, S.P. Shah, Basic Concepts and Mechanical Properties: Tension, Fiber-Reinforced Cement Composites, McGraw-Hill, New York, NY, USA, (1992) 37-84.
[6] A. Amin, S.J. Foster, A. Muttoni, derivation of the σ-w relationship for sfrc from prism bending tests, Struct. Concr. 16 (1) (2015) 93–105.
[7] Eduardo B. Pereira, Gregor Fischer, Joaquim A. O. Barros, Direct assessment of tensile stress-crack opening behavior of Strain Hardening Cementitious Composites (SHCC), Cement and Concrete Research, (2012) Vol. 42, Issue 6, pp.834-846.
[8] Jing Yu, Christopher K. Y. Leung, Novel experimental method to determine crack-bridging constitutive relationship of SHCC using digital image processing, Strain-Hardening Cement-Based Composites SHCC-4, Springer, Dresden, Germany, (2018) Vol. 15, pp.55-62.
[9] V.C. Li, Micromechanics of crack bridging in fibre-reinforced concrete, Mater. Struct. 26 (1993) 486–494.
[10] F. Laranjeira, Design-oriented Constitutive Model for Steel Fiber Reinforced Concrete, Universitat Politècnica de Catalunya, Spain, PhD-thesis, (2010).
[11] En-Hua Yang, Shuxin Wang, Yingzi Yang, Victor C. Li, Fiber-bridging constitutive law of engineered cementitious composites, J. Adv. Concr. Technol. 6 (1) (2008) 181–193.
[12] T. Kanakubo, M. Miyaguchi, K. Asano, Influence of fiber orientation on bridging performance of polyvinyl alcohol fiber-reinforced cementitious composite, Mater. J. American Concr. Inst. 113 (2) (2016) 131–141.
[13] T. Kanakubo, S. Echizen, J. Wang, Y. Mu, Pullout behavior of bundled aramid fiber in fiber-reinforced cementitious composite, Mater. 13 (7) (2020) 1746.
[14] Y. Ozu, M. Miyaguchi, T. Kanakubo, Modeling of bridging law for PVA fiber-reinforced cementitious composites considering fiber orientation, J. Civil Eng. Archi. 12 (2018) 651–661.
[15] T. Kanakubo, N. Yamato, Crack width prediction method for steel and FRP reinforcement based on bond theory, J. Adv. Concr. Technol. 12 (2014) 310–319.
[16] J. Deluce, S.C. Lee, F.J. Vecchio, "Crack formation in FRC structural elements containing conventional reinforcement." In: G. J. Parra-Montesinos, A. E. Naaman and H. W. Reinhardt, Eds. Proc 6th international RILEM Workshop on High Performance Fiber Reinforced Cement Composites (HPFRCC6), Michigan, USA, (2012) June 19-22, 2011, Dordrecht, Germany: Springer, 271-278.
[17] M. Kunieda, M. Hussein, N. Ueda, H. Nakamura, Enhancement of crack distribution of UHP-SHCC under axial tension using steel reinforcement, J. Adv. Concr. Technol. 8 (1) (2010) 49–57.
[18] G. Fischer, V.C. Li, Influence of matrix ductility on tension-stiffening behavior of steel reinforced engineered cementitious composites (ECC), Struct. J. American Concr. Inst. 99 (1) (2002) 104–111.
[19] H. Ogura, M. Kunieda, H. Nakamura, Tensile fracture analysis of fiber reinforced cement-based composites with rebar focusing on the contribution of bridging forces, J. Adv. Concr. Technol. 17 (2019) 216–231.
[20] H. Stang, T. Aarre, Evaluation of crack width in frc with conventional reinforcement, Cem. Concr. Compos. 14 (1992) 143–154.

[21] A. Amin, R.I. Gilbert, Instantaneous crack width calculation for steel fiber-reinforced concrete flexural members, Struct. J. American Concr. Inst. 115 (2) (2018) 535–543.
[22] K. Asano T. Kanakubo , Study on Size Effect in Bond Splitting Behavior of ECC, Bond in Concrete 2012, Volume 2 Bond in New Materials and under Severe Conditions, (2016) 855–859.
[23] Y. Ozu, K. Watanabe, A. Yasojima, T. Kanakubo, Evaluation of Size Effect in Bending Characteristics of DFRCC Based on Bridging Law, ACF 2016, The 7th International Conference of Asian Concrete Federation, 3. Concrete structures, Paper No.32 (2016).